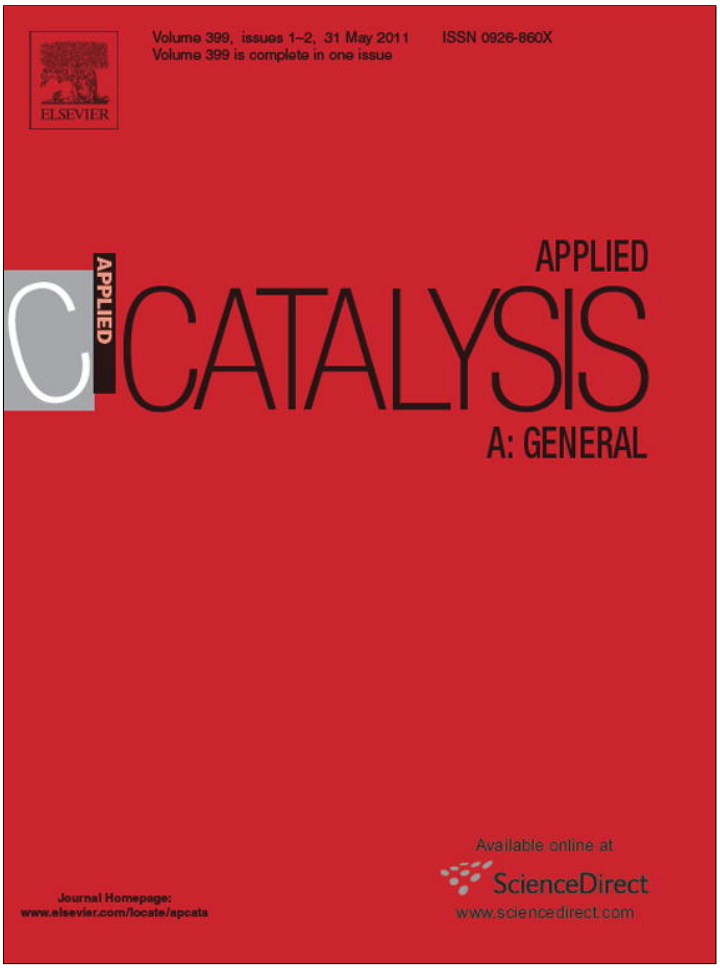

Applied Catalysis A: General 399 (2011) 146–153

Contents lists available at ScienceDirect

Applied Catalysis A: General

journal homepage: www.elsevier.com/locate/apcata

MgO-based catalysts for monoglyceride synthesis from methyl oleate and glycerol: Effect of Li promotion

C.A. Ferretti, C.R. Apesteguía, J.I. Di Cosimo*

Catalysis Science and Engineering Research Group (GICIC)-INCAPE (UNL-CONICET) Santiago del Estero 2654, (3000) Santa Fe, Argentina

ARTICLE INFO

Article history:
Received 12 January 2011
Received in revised form 24 March 2011
Accepted 28 March 2011
Available online 1 April 2011

Keywords:
Glycerolysis
Monoglyceride
Glycerol
Fatty acid methyl ester
Base catalysis

ABSTRACT

The synthesis of monoglycerides (glyceryl monooleates) by heterogeneously catalyzed glycerolysis of an unsaturated fatty acid methyl ester (methyl oleate) was studied on MgO and Li-promoted MgO catalysts.

Several MgO-based catalysts with different Li loadings were prepared by incipient wetness impregnation and characterized by XRD, N_2 physisorption, and FTIR and TPD of CO_2 among other techniques. Promotion of MgO with lithium, a basic promoter, affected the textural and structural properties of the resulting oxides so that more crystalline MgO phases with decreased surface area were obtained at increasing Li contents. Furthermore, the addition of Li generated new strong base sites because of formation of dispersed surface Li_2O species, and thereby increased the total base site density of parent MgO.

Li-containing MgO catalysts efficiently promoted the glycerolysis reaction, achieving high monoglyceride yields (70–73%) at 493 K. The initial monoglyceride formation rate increased linearly with the Li content on the sample following the enhanced overall catalyst base strength. Although conversions at the end of the run were ≈100% for all the catalysts, the monoglyceride selectivity slightly decreased with the Li loading, probably as a consequence of the less surface affinity for glycerol adsorption that facilitates competing monoglyceride re-adsorption and transformation to diglycerides by consecutive glycerolysis or disproportionation reactions.

1. Introduction

Biodiesel is a biomass-derived fuel for supplementation or potential replacement of non-renewable petroleum diesel. Interest in biodiesel production is growing worldwide because of the increasing consumption and price of fossil fuels. According to the International Energy Agency if recent demand and production trends continue, world production of biodiesel could exceed 18 million tons per year by 2012.

Currently, biodiesel is produced by transesterification of triglycerides found in plant oils and animal fats. Glycerol (Gly) is the main co-product in the biodiesel synthesis process, representing 10% of the biodiesel production. Therefore, the increasing production of biodiesel around the world generates a Gly surplus that is becoming a matter of economic and environmental concern since the Gly price drop has forced the producers to burn or sell it without refining. Thus, new applications intended to convert Gly into value-added chemicals are highly desirable not only to improve the economics of biodiesel production but also for ecological reasons.

In addition to the traditional uses of Gly in the formulation or synthesis of food, cosmetic and pharmaceutical products, liquid detergents and antifreeze [1], applications of Gly for the production of hydrogen [2], liquid fuels [3], fuel additives [4] and chemicals [1,5,6] have been lately claimed. In this regard, the monoglyceride (MG) synthesis by transesterification (glycerolysis) of fatty acid methyl esters (FAME) with Gly, Scheme 1, as an attractive option to transform Gly into fine chemicals.

Monoglycerides, the glycerol monoesters of fatty acids, are molecules consisting of a hydrophilic head and a hydrophobic tail having surfactant and emulsifying properties that find application in food, detergent, plasticizer, cosmetic and pharmaceutical formulations [5,7]. The commercial liquid-catalyzed synthesis route to produce MG involves strong mineral bases such as $Ca(OH)_2$ and KOH; the process entails concerns related to corrosion and disposal of spent base materials. In addition, the homogeneously catalyzed route gives reaction products containing only 40–60% MG, the rest being diglycerides (DG) and triglycerides (TG). Several purification steps are required to obtain food or pharmaceutical grade MG, such as neutralization of the

* Corresponding author. Tel.: +54 342 4555279; fax: +54 342 4531068.
E-mail address: dicosimo@fiq.unl.edu.ar (J.I. Di Cosimo).

0926-860X/$ – see front matter © 2011 Elsevier B.V. All rights reserved.
doi:10.1016/j.apcata.2011.03.051

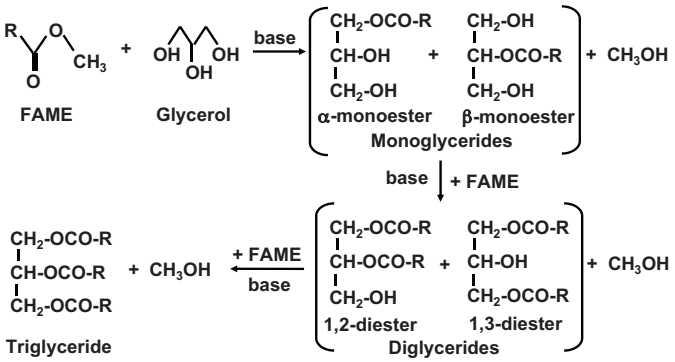

Scheme 1. Monoglyceride synthesis via transesterification (glycerolysis) of a fatty acid methyl ester (FAME) with glycerol and consecutive reactions to diglycerides and triglycerides.

reaction media and discoloration followed by expensive molecular distillation [5,7].

The heterogeneously catalyzed process for MG synthesis presents environmental and practical advantages but its industrial implementation to efficiently replace the current technology using liquid bases is still a challenge. In previous work [8,9] we studied the glycerolysis of an unsaturated FAME, methyl oleate (C18:1), using solid catalysts with different acid–base properties. We investigated the experimental conditions required to operate in a kinetically controlled regime and discussed the optimization of reaction parameters for improving MG yield [9]. Moreover, the chemical nature and the acid-base requirements of the active site for promoting the MG synthesis were investigated using single oxide solid catalysts with different electronegativities. A good correlation was found between the catalytic activity and the base site number. In addition, we concluded that glycerolysis of methyl oleate requires strong base sites such as the coordinatively unsaturated oxygen anions present on the surface of MgO [8].

In this paper we continue our investigations on the heterogeneously catalyzed glycerolysis of methyl oleate. We focus on MgO-based catalysts and study the effect of the addition of basic promoters such as Li on the MgO structure and surface base properties. The Li-MgO catalysts were then tested in the FAME glycerolysis reaction in order to correlate the activity and selectivity to MG with the sample Li loading.

2. Material and methods

2.1. Catalyst synthesis

Solids used were MgO (Carlo Erba 99%; 27 m^2/g), Li(OH) (anhydrous, Johnson Matthey 99.3%) and Li_2CO_3 (Puratronic 99.99%).

High surface area magnesium oxide was prepared by hydration with distilled water of low-surface area commercial MgO. Then the resulting $Mg(OH)_2$ was decomposed and stabilized in a N_2 flow for 1 h at 373 K, then for 1 h at 623 K, and finally for 18 h at 773 K to obtain a catalyst with a surface area 10 times higher than that of the original MgO [10]. The catalyst was finally ground and sieved, and the particles with average particle size of 177–250 μm were used for the catalytic experiments.

A set of lithium-promoted MgO samples was prepared by incipient wetness impregnation. Lithium was added to the high surface area MgO using a hydroxide aqueous solution containing the required Li concentration to obtain catalysts with 0.09, 0.17, 0.30, 0.54 and 0.94 wt% of lithium. After incorporation of the Li promoter, all samples were dried at 353 K and finally decomposed and stabilized at 773 K during 18 h in flowing N_2. The Li-doped MgO samples were identified as Li/MgO-x (x = 09, 17, 30, 54 and 94).

2.2. Catalyst characterization

BET surface areas were determined by N_2 physisorption at 77 K in a NOVA-1000 Quantachrome sorptometer. Pore size distributions were estimated by the Barrett-Joyner-Halenda (BJH) method within the pore diameter range of ≈10–300 Å; total pore volumes were also measured during the analysis. Li content of the samples was measured by atomic absorption spectrometry (AAS).

The structural properties of solid samples were determined by X-ray diffraction (XRD) using a Shimadzu XD-D1 instrument.

Catalyst basic properties were measured by temperature-programmed desorption (TPD) and infrared spectroscopy (IR) of CO_2. For the CO_2 TPD experiments, samples were pretreated in situ in a N_2 flow at 773 K, cooled down to room temperature, and then exposed to a flowing mixture of 3% of CO_2 in N_2 until surface saturation was achieved (5 min). Weakly adsorbed CO_2 was removed by flushing with N_2. Finally, the temperature was increased to 773 K at a ramp rate of 10 K/min. The flow containing the desorbed CO_2 was passed through a methanation reactor and converted to CH_4 on a Ni/Kieselghur catalyst at 673 K; CH_4 was then continuously analyzed using a flame ionization detector (FID). Efficiency of the CO_2 conversion in CH_4 was checked periodically by introducing known amounts of CO_2 and CH_4 in the methanation reactor. The same setup was used for the carbonate temperature-programmed decomposition (TPDe) experiments. Samples were pretreated at 673–773 K, cooled down to room temperature, and then heated up to 973 K at a ramp rate of 10 K/min in a N_2 flow. The evolved CO_2 was converted to CH_4 in the methanation reactor and analyzed by FID.

The chemical nature of adsorbed surface CO_2 species was determined by IR after CO_2 adsorption at room temperature and sequential evacuation at increasing temperatures. Samples were pressed in a wafer and degassed in vacuum at 773 K for 1 h and then cooled down to room temperature. The spectrum of the pretreated catalyst was then taken. After admission of 5 kPa of CO_2 and evacuation at 298, 373, 473 and 573 K, the CO_2 adsorption spectra were recorded at room temperature. Spectra of the adsorbed species were obtained by subtracting the catalyst spectrum. Data were collected in a Shimadzu FTIR Prestige-21 spectrometer using an inverted T-shaped cell fitted with CaF_2 windows containing the sample pellet. The absorbance scale was normalized to 20 mg.

2.3. Catalytic tests

The transesterification of methyl oleate (oleic acid methyl ester, Fluka, >60%, with 86% total C18 + C16 esters as determined by gas chromatography), with glycerol (Aldrich, 99%,) was carried out at 493 K in a seven-necked cylindrical glass reactor with mechanical stirring equipped with a condenser to remove the methanol generated during reaction. In the text FAME and Gly stand for methyl oleate and glycerol, respectively.

A Gly/FAME molar ratio of 4.5 and a catalyst/FAME ratio (W_{cat}/n^0_{FAME}) of 30 g/mol were used. The reactor was operated in a batch regime at atmospheric pressure under flowing N_2 (35 mL/min). First, the liquid reactants were introduced and the reactor was flushed with nitrogen, then they were heated to reaction temperature under stirring (700 RPM). Catalyst was pretreated ex-situ at 773 K for 6 h to remove adsorbed water and carbon dioxide and kept overnight at 373 K in flowing N_2 until used, then quickly transferred to the reactor without exposing it to air to start the reaction. The reactor was assumed to be perfectly mixed.

The reaction products α- and β-glyceryl monooleates (MG), 1,2- and 1,3-glyceryl dioleates (diglycerides, DG) and glyceryl trioleate (triglyceride, TG) were analyzed by gas chromatography (GC) after silylation to improve compound detectability [11]. Details are given elsewhere [8,12]. Other reaction products were diglycerols (DGly)

Table 1
Physicochemical properties of Li/MgO-*x* and MgO catalysts.

Catalyst	Li^+ loading[a] (wt%)	Monolayer coverage fraction, $m^2_{Li_2O}/m^2_{MgO}$, (%)	Surface area, S (m^2/g)	Pore volume, v_g (cm^3/g)	Mean pore size[b] (Å)	XRD analysis	
						Lattice parameter, ***a*** (Å)	Crystallite size (Å)
MgO	–	–	260	0.39	60	4.221	77
Li/MgO-09	0.09	1.3	203	0.32	64	4.243	88
Li/MgO-17	0.17	2.4	220	0.30	55	4.221	151
Li/MgO-30	0.30	4.3	188	0.27	58	4.214	121
Li/MgO-54	0.54	7.6	155	0.32	83	4.220	139
Li/MgO-94	0.94	13.3	26	0.08	123	4.208	207

[a] by AAS.
[b] mean diameter calculated with the Wheeler's equation as $4\,v_g/S$.

and triglycerols (TGly). Silylated samples were analyzed in a SRI 8610C gas chromatograph equipped with a flame ionization detector (FID), on-column injector port and a HP-1 Agilent Technologies 15 m × 0.32 mm × 0.1 μm capillary column.

Quantification was carried out using authentic standards of glyceryl trioleate (Sigma, 65%) and a commercial mixture of glyceryl mono and dioleate of known composition (Fluka, 71.5% MG and 25.3% DG).

FAME conversion (X_{FAME}, referred to the total content of esters in the reactant), selectivity (S) and yield (Y) were calculated through the following equations (n_j, mol of compound j; MG = monoglycerides (total of both isomers), DG = diglycerides (total of both isomers), TG = triglyceride):

$$X_{FAME}(\%) = \frac{n_{MG} + 2n_{DG} + 3n_{TG}}{n_{MG} + 2n_{DG} + 3n_{TG} + n_{FAME}} \times 100$$

$$S_{MG}(\%) = \frac{n_{MG}}{n_{MG} + 2n_{DG} + 3n_{TG}} \times 100$$

$$S_{DG}(\%) = \frac{2n_{DG}}{n_{MG} + 2n_{DG} + 3n_{TG}} \times 100$$

$$S_{TG}(\%) = \frac{3n_{TG}}{n_{MG} + 2n_{DG} + 3n_{TG}} \times 100$$

$$Y_j(\%) = \frac{X_{FAME}(\%)S_j(\%)}{100}$$

3. Results and discussion

3.1. Chemical, textural, and structural characterization of Li-promoted MgO catalysts

After hydration of commercial MgO and subsequent decomposition and stabilization at 773 K, the BET surface increased from 27 to 260 m^2/g due to the development of a porous structure because of gaseous evolution during $Mg(OH)_2$ decomposition. The chemical composition, BET surface area and XRD analysis of Li-promoted MgO (Li/MgO-*x*) and MgO catalysts activated at 773 K are presented in Table 1. Elemental analysis of the promoted oxides revealed Li loadings ranging between 0.09 and 0.94 wt%. Promotion with Li gradually decreased the catalyst surface area for Li loadings < 0.6 wt% (Table 1) but this effect was more severe at higher loadings. A similar effect on the MgO textural properties upon promotion with IA metals was reported previously [10,13]. The pore size distribution was also affected by Li doping so that the mean pore diameter increased with increasing the Li content from 60 Å in the parent MgO to twice as much in the Li/MgO-94 sample (123 Å).

Calculations of the promoter surface coverage carried out by considering that the lithium species after catalyst calcination is Li_2O indicated that the MgO surface (260 m^2/g) would be covered by one monolayer of Li_2O for Li loadings of about 7.1 wt%. Li loadings < 0.6 wt% in Li/MgO-*x* samples are below the monolayer saturation coverage, representing a fraction less than 10% of the MgO surface, Table 1, column 3. The low Li_2O coverage indicates that the lithium species in that compositional range are probably well dispersed on the MgO surface. At Li loadings > 0.6 wt%, the final surface area of the promoted oxide was about 1/10 that of the parent MgO and probably the actual Li_2O monolayer coverage fraction was much higher than the calculated in Table 1 (13.3%).

X-ray diffractograms of Li/MgO-*x* catalysts (not shown here) did not reveal the presence of any crystalline Li-containing phase; only a single phase of MgO periclase was detected regardless of the Li loading. The crystallite sizes of the MgO phase in the MgO and Li/MgO-*x* catalysts were determined from XRD patterns using the Scherrer equation for the reflection at $2\theta = 42.7^\circ$ and are given in Table 1. As a general trend, MgO crystallite size increased with increasing Li loading, in agreement with the sample surface area drop. This sintering effect is probably a consequence of the catalyst preparation procedure employed. In fact, after MgO impregnation with aqueous Li(OH) solutions the sample was heated in order to decompose the resulting $Li(OH)/Mg(OH)_2$ solid but at ≈700 K, previously to reach the decomposition temperature, Li(OH) melting occurs and particle agglomeration is expected to take place [14,15].

The unit cell parameter ***a*** of the MgO structure with face-centered cubic symmetry was calculated for Li/MgO-*x* catalysts from the corresponding X-ray diffractograms and is presented in Table 1. Since the ionic radius of Li^+ in Li_2O ($r_{Li^+} = 0.73$ Å) is slightly smaller than that of Mg^{2+} in MgO ($r_{Mg^{2+}} = 0.86$ Å) substitution of Li^+ for Mg^{2+} in the periclase structure might take place causing both, contraction of the MgO lattice and formation of strongly basic anionic vacancies. This would be more likely expected in low Li loading samples such as in Li/MgO-09 (0.09 wt% Li) because, as we demonstrated previously [13], the MgO promotion with higher Li loadings does not cause structural modifications of the periclase phase other than the increase of the crystallite size. However, according to the ***a*** values of Table 1 no detectable contraction of the MgO matrix has occurred at any Li doping level. Therefore, structural periclase promotion is ruled out; the Li^+ cations are located on the surface of Li/MgO-*x* samples probably forming small amorphous Li_2O or Li_2CO_3 domains, rather than being located inside the MgO matrix.

3.2. Surface base properties of Li-promoted MgO catalysts

As stated above, the fact that the Li loadings in Li/MgO-*x* catalysts were lower than the monolayer saturation coverage, suggests that the promoter species are highly dispersed on the MgO surface, probably affecting the basicity of the resulting promoted oxides. The basic properties of these samples were investigated using CO_2 as a probe molecule; a measure of the number and structure of

Table 2
Surface base site properties of MgO and Li/MgO-x samples by TPD of CO_2.

Catalyst	Total evolved CO_2, N_b (μmol/g)	Bulk carbonates[a] (μmol/g)	Base site density (μmol/m^2)			
			Total, n_b	Weak, n_{OH}	Medium, n_{MO}	Strong, n_O
MgO	516	0	2.0	0.3	0.7	1.0
Li/MgO-09	549	35	2.5	0.3	0.6	1.6
Li/MgO-17	586	49	2.4	0.2	0.5	1.7
Li/MgO-30	616	94	2.8	0.3	0.3	2.2
Li/MgO-54	791	167	4.0	0.4	0.8	2.8
Li/MgO-94	698	312	14.8	1.8	3.6	9.4

[a] CO_2 evolutions above 650 K.

chemisorbed CO_2 species was obtained by combining TPD and FTIR measurements of preadsorbed CO_2.

The CO_2 desorption rate as a function of sample temperature is shown in Fig. 1 for MgO and Li-MgO-*x* catalysts. The total evolved CO_2 (N_b, μmol/g) was obtained by integration of TPD curves and the resulting values are reported in Table 2. The N_b values show that the amount of evolved CO_2 from MgO is lower than from the Li/MgO-*x* catalysts; N_b progressively increased with the Li loading reaching a maximum for sample Li/MgO-54 and clearly decreased at higher loadings due to sintering of the MgO structure, as explained above. The observed N_b increase with Li content is in agreement with previous work on Li-promoted MgO catalysts [13], and indicates an enhanced number of surface oxygen species able to interact with CO_2 upon promotion.

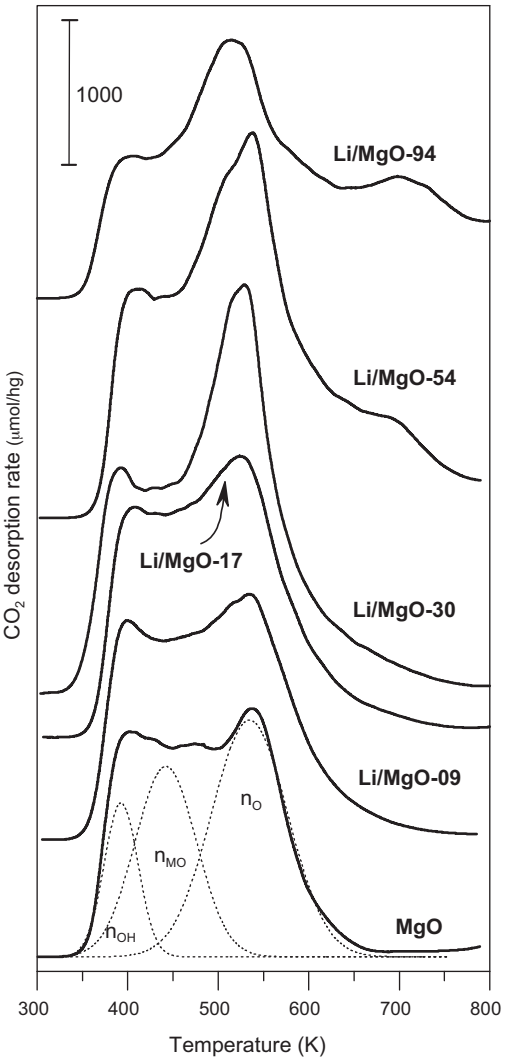

Fig. 1. TPD of CO_2 on MgO and Li/MgO-*x*.

The TPD profiles of Fig. 1 show that CO_2 desorbed in a broad temperature range, between 350 and 650 K, suggesting that the surfaces of both MgO and Li-promoted MgO catalysts contain several types of oxygen species that chemisorb CO_2 with different coordination and binding energy. The shape of the TPD traces changed at increasing Li loadings. In particular, the contribution of the high-temperature CO_2 desorption peak at ≈550 K increased with the Li content, thereby revealing that promotion with Li^+ generates new strong base sites.

In previous work [10,13], we explained the effect of alkaline metal promoters on the MgO basic properties by considering that the basicity of an oxide surface is related to the electro-donating properties of the combined oxygen anions, so that the higher the partial negative charge on the combined oxygen anions, the more basic the oxide. Therefore, surface promotion with more basic Li_2O oxide is expected to increase the overall basicity of MgO. Another feature of the TPD traces of Fig. 1 is the release of CO_2 above 650 K, which is more noticeable in samples with Li loadings ≥0.3 wt%.

To investigate the chemical nature of the surface base sites (oxygen anions) in MgO and Li-promoted catalysts, IR spectra of CO_2 adsorbed at room temperature were taken after sequential evacuation at increasing temperatures. Fig. 2 shows the carbonate region (1900–1100 cm^{-1}) of the spectra after evacuation at 298, 373, 473 and 573 K for MgO and Li/MgO-30 catalysts. In previous work by FTIR of CO_2 [13,16] on similar MgO-based catalysts we identified at least three CO_2 adsorption species: bicarbonate formed on OH^- groups (weak base sites), bidentate carbonate (B.C.) formed on M^{n+}–O^{2-} pairs (M^{n+} = Mg^{2+} or Li^+) located on surface steps (medium strength base sites) and unidentate carbonate (U.C.) formed on low coordination O^{2-} located in corners or edges (strong base sites). The bicarbonate bands (C–OH bending mode at 1220 cm^{-1}, symmetric and asymmetric O–C–O stretching modes at 1480 cm^{-1} and 1650 cm^{-1}, respectively) completely disappeared after evacuation at 373 K whereas U.C. (symmetric O–C–O stretching at 1360–1400 cm^{-1} and asymmetric O–C–O stretching at 1510–1560 cm^{-1}) and B.C. species (symmetric O–C–O stretching at 1320–1340 cm^{-1} and asymmetric O–C–O stretching at 1610–1650 cm^{-1}) remained on the surface. In summary, CO_2 adsorption on MgO and Li/MgO-30 forms carbonates in which surface oxygen anions with different coordination, i.e., with different basic properties, participate.

Fig. 2 shows that after evacuation at 573 K almost no CO_2 was retained on the surface of MgO, whereas the Li/MgO-30 sample still contained the bands of unidentate carbonates (U.C.). Consistent with the CO_2 TPD curves in Fig. 1, this result reveals that promotion with Li^+ generates stronger base sites. On the other hand, Fig. 2 clearly shows that the areas under the carbonate bands for the Li/MgO-30 sample were much higher than those of MgO. However, the N_b value determined on LiMgO-30 was only about 20% higher than that corresponding to MgO (Table 2), suggesting that Li/MgO-

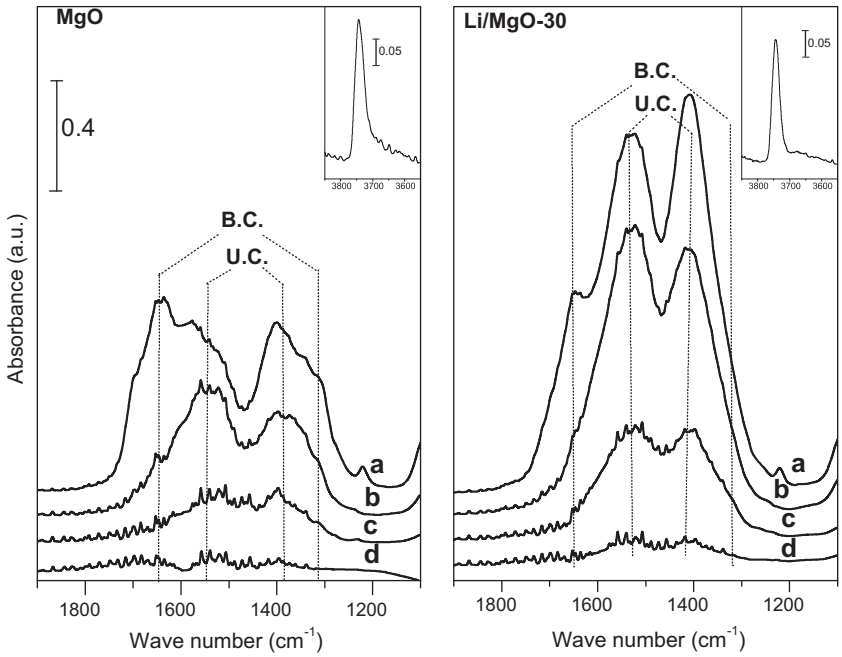

Fig. 2. FTIR spectra of CO_2 adsorbed species on MgO and Li/MgO-30 after evacuation at increasing temperatures. (a) 298 K; (b) 373 K; (c) 473 K; (d) 573 K [CO_2 adsorption at room temperature; B.C: bidentate carbonate; U.C: unidentate carbonate]. Inset: OH region of the catalyst spectrum before CO_2 adsorption.

30 would contain stable bulk carbonates that are detectable in the IR spectra but that do not release significant amounts of CO_2 in the temperature range used for TPD experiments.

To elucidate whether the CO_2 evolutions in Fig. 1 arise from surface adsorbed CO_2 or from decomposition of bulk carbonates, additional investigations were carried out combining TPD of CO_2 and TPDe experiments for MgO, Li/MgO-94 and commercial Li_2CO_3, Fig. 3. Although MgO and Li/MgO-94 formed bulk carbonates the latter contained a much stable species and in a higher concentration, in agreement with the IR results (curves MgO-TPDe and Li/MgO-94-TPDe in Fig. 3).

The CO_2 TPD of Li_2CO_3 (curve Li_2CO_3-TPD in Fig. 3) presented not significant CO_2 desorption at 300–650 K, i.e., at the typical temperature range of the TPD experiments of Fig. 1, showing only a small peak at 400 K. Therefore, in Fig. 1, the CO_2 TPD signals evolved at 300–650 K correspond to CO_2 released from the surface base sites of MgO and Li_2O and not to desorption from Li_2CO_3.

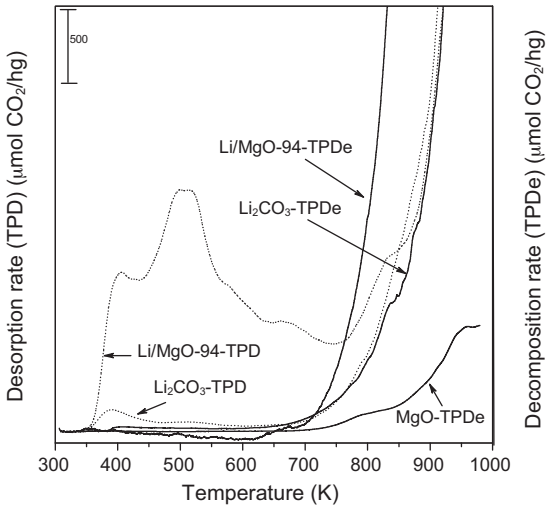

Fig. 3. TPD of CO_2 on Li/MgO-94 and Li_2CO_3 samples (dotted lines); Carbonate decomposition (TPDe) of MgO, Li/MgO-94 and Li_2CO_3 samples (solid lines).

In particular, the peak at ≈550 K in the CO_2 TPD traces (Fig. 1) that increases with the Li loading, was assigned to CO_2 desorption from the strongly basic oxygen anions associated to reactive surface lithium species.

On the other hand, the CO_2 TPD peak at ≈700 K, that increases with Li loading (Fig. 1), is probably due to decomposition of three-dimensional Li_2CO_3 that starts melting and decomposing at that temperature forming Li_2O and CO_2 at about 1000 K (curve Li_2CO_3-TPDe in Fig. 3) [14]. Other authors have already observed that the decomposition of Li_2CO_3 in Li-MgO samples peaks at 933 K [17].

Based on the information of Figs. 2 and 3, the CO_2 TPD profiles of Fig. 1 were deconvoluted in three desorption bands, reaching maximum desorption rates at about 400, 450, and 550 K. Although CO_2 desorption follows first-order kinetics, for simplicity we have used Gaussian functions for the deconvolution and integration of the TPD traces. The CO_2 evolutions above 650 K, which were assigned to decomposition of highly stable three-dimensional (bulk) carbonates, were not taken into account for quantifying the number of basic sites. Nevertheless, the amounts of CO_2 evolved above 650 K were included in Table 2, column 3. The base site densities in μmol/m^2, either total or the contribution of each basic species, were calculated then from the integrated areas of the TPD experiments after correcting by the surface area and assuming a CO_2:surface base site = 1:1 desorption stoichiometry. The total base site density (n_b) and the contribution of each band, identified as the density of weak (n_{OH}), medium (n_{MO}) and strong (n_O) base sites, respectively, are reported in Table 2. The n_b values notoriously increased with the Li loading as well as the contribution of strong base sites (n_O), thereby confirming that Li promotion generated more base sites and enhanced the catalyst average base strength.

3.3. General features of the methyl oleate (FAME) glycerolysis on MgO

All the Mg-based catalysts were tested in the transesterification of FAME with Gly in a batch reactor consisting of four phases [9]: the solid catalyst; the bottom liquid layer formed by the Gly phase; the top liquid fatty phase containing FAME and glyceride products, and

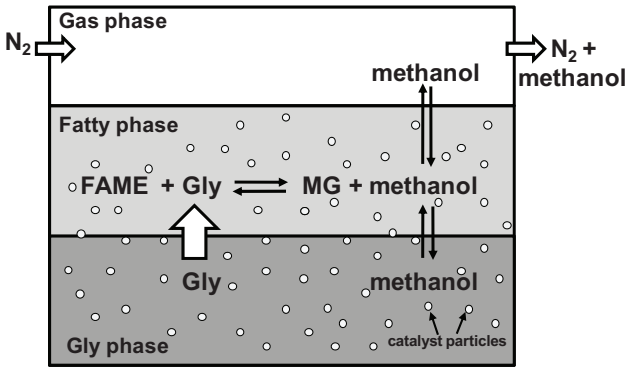

Scheme 2. Four-phase reactor for the heterogeneously catalyzed monoglyceride synthesis.

the gas phase containing methanol that is continuously removed from the reactor. The reactor is depicted in Scheme 2. Since FAME is not soluble in Gly and Gly is barely soluble in the FAME phase, the reaction occurs in the top phase where both reactants may coexist. Thus, Gly has to be transferred from the bottom phase to the FAME phase where it is immediately consumed. For this reason, all the catalytic experiments were carried out with excess Gly. The Gly concentration in the FAME phase increases during reaction because the surfactant properties of glyceride products enhance Gly solubility in the FAME phase. On the other hand, glycerides were never found in the Gly phase under our heterogeneous catalysis conditions.

In previous work [9] we investigated the operative conditions required to rule out diffusional limitations in this four-phase reaction system. Only mass-transfer limitations were investigated since the calculated reaction enthalpy for monoglyceride formation was very low (0.28 kJ/mol). We concluded that at the reaction temperature range under study (473–523 K), using catalyst particles of 177–250 μm and stirring rates of 400–700 rpm., the main reaction is kinetically controlled.

Fig. 4 shows a catalytic experiment carried out with MgO at typical reaction conditions (493 K) where the predominant formation of monoglycerides can be observed with α-MG being the main isomer over β-MG. Also, diglycerides formed by consecutive transesterification (Scheme 1) appeared mainly as 1,3-DG and to a lesser extent as 1,2-DG. No TG formation was detected at any reaction condition. The preferential formation of α-MG respect to β-MG and that of 1,3-DG compared to 1,2-DG is possibly a consequence of the

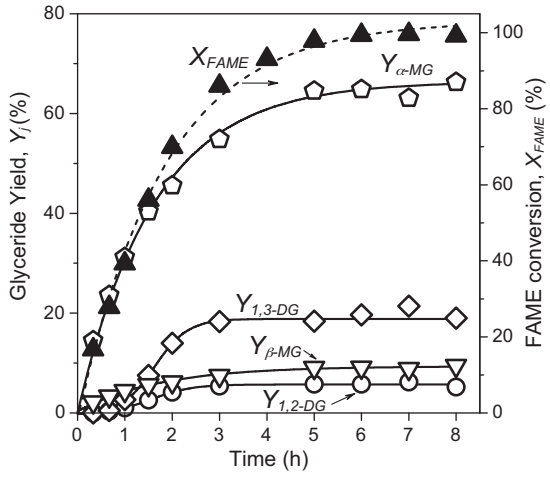

Fig. 4. FAME conversion (X_{FAME}) and glyceride product yield (Y) as a function of reaction time [MgO; T = 493 K; Gly/FAME = 4.5].

$$2\,Gly \underset{}{\overset{I}{\rightleftharpoons}} DGly + H_2O$$
$$DGly + Gly \overset{II}{\rightleftharpoons} TGly + H_2O$$
$$2\,MG \overset{III}{\rightleftharpoons} DG + Gly$$

Scheme 3. Secondary reactions I and II: polyglycerol formation by etherification reactions; III: disproportionation reaction.

higher accessibility and number of primary OH groups in the Gly molecule. The non-zero initial slope (slope at $t = 0$) of the $Y_{\beta\text{-MG}}$ vs time curve of Fig. 4 suggests that β-MG is a primary product of the glycerolysis reaction formed catalytically and directly from FAME and not consecutively from α-MG by acyl migration as occurs in enzymatic catalysis [18,19]. On the contrary, the zero initial slope of the $Y_{1,2\text{-DG}}$ and $Y_{1,3\text{-DG}}$ curves indicates consecutive formation from α- and β-MG. However, isomer interconversion at higher reaction times cannot be ruled out, neither the existence of disproportionation reactions [9]. In addition, the plateau of the Y_j curves at $t > 6$ h, which is more evident for the secondary DG products, is due to the total conversion of FAME that decelerates essentially the secondary reaction and not to diffusional limitations or catalyst deactivation.

On the other hand, at 100% FAME conversion the total MG/total DG ratio measured at 493 K was ≈3, a much higher value than that currently obtained during the homogeneously catalyzed commercial process (≈0.7–1.5) [7].

3.4. Effect of Li promotion on the MgO activity and selectivity for the FAME glycerolysis reaction

MgO and Li/MgO-*x* samples were tested in the methyl oleate glycerolysis reaction at 493 K using a reactant mixture of Gly/FAME = 4.5 (molar ratio) and a catalyst/reactant ratio (W_{cat}/n^0_{FAME}) of 30 g/mol. The main effect of Li loading was the improvement of the catalyst activity. Indeed, Fig. 5A shows that the reaction time required to reach 100% FAME conversion decreased with the Li content on the sample; for example, complete FAME conversion on MgO and Li/MgO-54 was reached in 6 h and 2 h, respectively. However, for the highest Li loading, sample Li/MgO-94, a deactivation process was observed since FAME conversion rapidly increased with time but then stabilized at about 97%. The experiment was interrupted after 4 h because of darkening and emulsification of the reactant mixture, probably because of the formation of polyglycerols from etherification reactions in the Gly phase [20], as sketched in reactions I and II of Scheme 3.

The incidence of Li leaching was also investigated. In particular, the liquid FAME and Gly phases (Scheme 2) were analyzed after reaction with Li/MgO-94; the Li concentration in the FAME phase, where the reaction occurs, was near the detection limit but the catalyst lost about 17% of the Li content in the Gly phase. These results are somewhat expected since lithium compounds are more soluble in polar substances [14]. Li species dissolved in the Gly phase probably favored polyglycerol formation.

In what concerns to selectivity, no TG was detected during the catalytic tests using Li-promoted catalysts with MG and DG being the only glyceride products formed during the 8-h experiments. In particular, the MG yields (Y_{MG}) obtained with the Li/MgO-*x* catalysts are presented in Fig. 5B. Samples with Li loadings ≥0.3 wt%, completely converted FAME in less than 3 h reaching at that time maximum Y_{MG} values of 65–70% which then decreased with the progress of the reaction because of DG formation, Fig. 5B. Conversion of MG to DG after complete FAME consumption cannot be explained by the reaction pathways depicted in Scheme 1 that entailed DG formation by consecutive MG reaction with FAME. Thus, the maximum of MG yield curves observed in Fig. 5B for

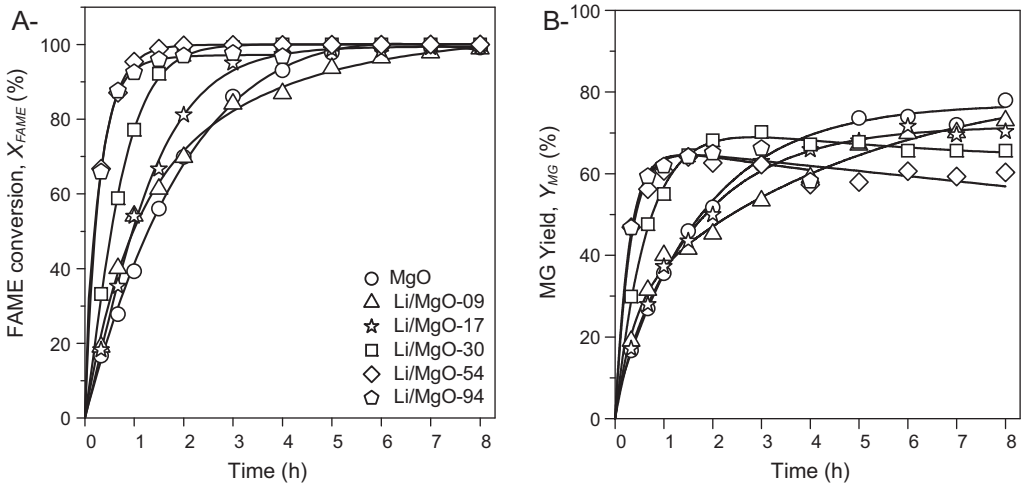

Fig. 5. FAME conversion (X_{FAME}), (A); Monoglyceride yield (Y_{MG}), (B). [MgO and Li/MgO-*x* catalysts; T = 493 K; Gly/FAME = 4.5].

high Li loading samples probably reflects the MG conversion via disproportionation reactions such as reaction III of Scheme 3.

In contrast, the Y_{MG} curves corresponding to low Li loading samples did not show a maximum during the experiment time frame, reaching values between 70 and 73% at the end of the runs, Fig. 5B.

The initial intrinsic MG formation rate (r^0_{MG}, h^{-1}) on the Li/MgO-*x* catalysts was evaluated on the basis of the base site density measured by TPD of CO_2 and calculated from the slopes of Y_{MG} vs. time curves of Fig. 5B as

$$r^0_{MG} = \left(\frac{n^0_{FAME}}{S n_b W_{cat}}\right)\left[\frac{dY_{MG}}{dt}\right]_{t=0}$$

The resulting values were plotted in Fig. 6 as a function of the Li loading. It is observed that Li promotion improved the intrinsic catalyst activity, so that the r^0_{MG} value measured on the sample with highest Li loading (Li/MgO-94) was five-fold higher than that on MgO.

In previous work [8] we investigated the catalytic performance of MgO calcined at different temperatures with the purpose to identify the chemical nature of the MgO active site that promotes the FAME glycerolysis reaction. We observed that an increase of the calcination temperature decreases the MgO average basic strength giving smoother catalyst surfaces with the consequent decrease of the contribution of low coordination oxygen anions (strong base sites) to the total basicity. We also found that the MgO activity for the glycerolysis reaction satisfactorily correlates with the density of strong base sites and we therefore concluded that the monoglyceride synthesis on MgO is mainly promoted on strong base sites.

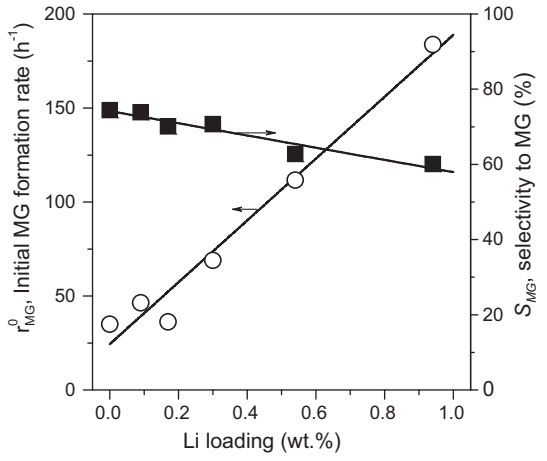

Fig. 6. Intrinsic initial MG formation rate (r^0_{MG}) and MG selectivity (S_{MG}) at 100% FAME conversion as a function of the Li loading of Li/MgO-*x* catalysts. Reaction conditions as in Fig. 5

The results of Fig. 6 are in line with this previous work since the linear increase of the intrinsic catalytic activity cannot be explained by just a quantitative change in n_b upon increasing the Li loading and therefore must be attributed to a qualitative modification of the surface properties such as the increase of the average basicity due to the enhanced contribution of strong base sites (n_O values in Table 2) in Li-containing catalysts.

The effect of the Li promotion on the reaction selectivity was also investigated. In Fig. 6, the selectivity to MG (S_{MG}) obtained when just reaching 100% FAME conversion was plotted as a function of Li loading. Results showed that Li promotion was in some way detrimental to monoglyceride selectivity since the S_{MG} value slightly but gradually decreased with the Li loading; qualitatively similar results were obtained at other conversion levels.

An explanation for the diminution of S_{MG} with Li loading observed in Fig. 6 is based on the preparation method of Li/MgO-*x* catalysts. The impregnation technique leads to an oxide composed mainly by MgO, which is in intimate contact with a small amount of Li^+ cations forming Li–O–Mg or Li–O–Li domains and Li_2CO_3 patches. Thus, upon lithium promotion, the original Mg–OH groups of the MgO surface were replaced by the Li-containing species probably giving rise to a more hydrophobic surface. In fact, the IR spectra in the OH region (3800–3600 cm^{-1}) taken for MgO and Li/MgO-30 after degassing at 573 K showed that the MgO surface was more hydroxylated, as shown as an inset graph in Fig. 2. Similar qualitative results were obtained by XPS in the O 1s region (not shown). On hydrophilic surfaces such as that of MgO, FAME adsorption is unlikely but Gly would remain strongly adsorbed hindering readsorption of MG molecules initially formed and avoiding their consecutive conversion to DG, thereby increasing MG selectivity.

4. Conclusions

MgO doping with increasing Li contents reduces the MgO surface area but increases its surface basicity because the addition of Li generates new low coordination O^{2-} anions that are strong base sites. Thus, Li promotion enhances both, the base site density and the average base strength.

The monoglyceride synthesis from methyl oleate and glycerol is efficiently catalyzed on MgO and Li-promoted MgO catalysts.

Monoglyceride yields of up to 73% are obtained on MgO and low-loading Li-promoted MgO (≤0.3 wt% Li) at 493 K in excess glycerol. Monoglyceride formation is promoted on strong base sites and thereby the intrinsic initial monoglyceride formation rate increases with the Li content in the sample.

In contrast, the addition of Li is slightly detrimental to monoglyceride selectivity, probably because Li-promoted MgO catalysts have a more hydrophobic surface than that of MgO and thus show less affinity for glycerol adsorption. A weaker glycerol adsorption on the catalyst surface would enable monoglyceride re-adsorption and its consecutive conversion to diglycerides.

Acknowledgements

Authors thank Universidad Nacional del Litoral (UNL), Consejo Nacional de Investigaciones Científicas y Técnicas (CONICET) and Agencia Nacional de Promoción Científica y Tecnológica (ANPCyT) of Argentina, for the financial support of this work. They also thank H. Cabral for technical assistance.

References

[1] A. Corma, S. Iborra, A. Velty, Chem. Rev. 107 (2007) 2411–2502.
[2] J.W. Shabaker, G.W. Huber, J.A. Dumesic, J. Catal. 222 (2004) 180–191.
[3] A. Corma, G.W. Huber, L. Sauvanaud, P. O'Connor, J. Catal. 247 (2007) 307–327.
[4] R.S. Karinen, A.O.I. Krause, Appl. Catal. A: Gen. 306 (2006) 128–133.
[5] Y. Zheng, X. Chen, Y. Shen, Chem. Rev. 108 (2008) 5253–5277.
[6] F. Jerome, Y. Pouilloux, J. Barrault, ChemSusChem 1 (2008) 586–613.
[7] A. Corma, S.B.A. Hamid, S. Iborra, A. Velty, J. Catal. 234 (2005) 340–347.
[8] C.A. Ferretti, A. Soldano, C.R. Apesteguía, J.I. Di Cosimo, Chem. Eng. J. 161 (2010) 346–354.
[9] C.A. Ferretti, R.N. Olcese, C.R. Apesteguía, J.I. Di Cosimo, Ind. Eng. Chem. Res. 48 (2009) 10387–10394.
[10] J.I. Di Cosimo, V.K. Díez, C.R. Apesteguía, Appl. Catal. A: Gen. 13 (1996) 149–166.
[11] W.H. Tallent, R. Kleiman, J. Lipid Res. 9 (1968) 146–148.
[12] C.A. Ferretti, "Valorización catalítica de glicerol: Síntesis de monoglicéridos". PhD Thesis, Universidad Nacional del Litoral, Santa Fe, Argentina, 2010.
[13] V.K. Díez, C.R. Apesteguía, J.I. Di Cosimo, J. Catal. 240 (2006) 235–244.
[14] P. Patnaik, Handbook of Inorganic Chemicals, McGraw-Hill, New York, (2003), p. 497, 502, 507 and 519.
[15] S. Noda, M. Nishioka, M. Sadakata, J. Phys. Chem. B 103 (1999) 1954–1959.
[16] J.I. Di Cosimo, V.K. Díez, M. Xu, E. Iglesia, C.R. Apesteguía, J. Catal. 178 (1998) 499–510.
[17] S.J. Korf, J.A. Roos, N.A. De Bruijn, J.G. Van Ommen, J.R.H. Ross, App. Catal. 58 (1990) 131–146.
[18] W. Li, W. Du, Q. Li, T. Sun, D. Liu, J. Molec. Catal. B: Enzym. 63 (2010) 17–22.
[19] J.C. Bellot, L. Choisnard, E. Castillo, A. Marty, Enzyme Microb. Technol. 28 (2001) 362–369.
[20] J. Clacens, Y. Pouilloux, J. Barrault, Appl. Catal. A: Gen. 227 (2002) 181–190.